Optica Applicata, Vol. XLI, No. 3, 2011

The interference characteristics of light-waves from a tilted and defocused cat-eye optical lens irradiated by laser beam

YANZHONG ZHAO[1*], HUAYAN SUN[1], XI ZHANG[1], YONG WANG[2]

[1]Academy of Equipment Command and Technology of PLA, Beijing, P.R. China

[2]Zhengzhou Air Defence Forces Academy of PLA, Zhenzhou, P.R. China

[*]Corresponding author: zhaoyan198@yahoo.cn

When a tilted and defocused cat-eye optical lens is irradiated by laser beam, the reflected light-waves can be regarded as an off-axis spherical wave. Based on this idea and the theory of angular spectrum, our research has been directed towards some formulas describing the interference of the cat-eye reflected light with the reference incidence light. Through numerical computation, relationships governing the variation of the interference characteristics with parameters including the incidence angle, the tilted angle of the moving mirror, and the focal shift, are established. The relationships are experimentally validated. Our results have shown that the interference circles gradually move outwards, and the spot profile becomes broken with the increase of the incidence angle, the coordinates of the curvature center of the interference fringes are proportional to the incidence angle and the tilted angle of the moving mirror, the number of the interference fringes becomes larger along with the increase of the focal shift and the tilted angle of the moving mirror. The results can be used to estimate the tilted state of the cat-eye target.

Keywords: interference characteristics, cat-eye effect, tilted and defocused cat-eye optical lens, incidence angle.

1. Introduction

Most optical lenses used in photoelectric equipment have detectors fixed on their focal plane, so the laser beam that irradiates on the photoelectric equipment can be reflected back by the optical lens along the entrance way [1–4]. Such phenomenon is defined as “cat-eye effect”, and such optical lenses are defined as “cat-eye optical lens”. This reflected theory is similar to that of cat’s eye reflector [5], which is widely used in laser tracking interferometer systems [6], adjustment-free lasers [7, 8], micro-displacement measurements [9], and free-space optical communications [10–12]. There are

some essential differences between cat's eye reflector and cat-eye optical lens. The cat's eye reflector is well designed, diffraction limited [5] and has little sensitivity to the direction of the incidence light [8], so it is a cooperative target in application. But the cat-eye optical lens is a non-cooperative target whose parameters are unknown. By using the active laser detection technique based on the theory of cat-eye effect of optical lens, a much larger detection distance and a higher orientation precision can be obtained than that by using passive detection technique [1, 2, 13]. But only little ordinary information can be acquired such as the location and distance of the target. The problem is that this is not enough for the latter information process system to give effective command, so we cannot decide whether to attack the target or not. If some parameters such as the incidence angle of the detected laser beam entering the target optical lens can be gained, we can know which location is being watched by the target optical lens. Therefore, we theorize that the cat-eye effect should be studied further to obtain some additional parameters of the optical target, and diffraction and interference characteristics of the cat-eye reflected light are the theoretical foundation for its application in recognition technique [14, 15].

The diffraction characteristics of the cat-eye reflected light have been studied some time [3, 4, 14, 15], but the interference characteristics of the cat-eye reflected light have never been studied to date. In addition, we consider the interferometry methods which are widely used in optical metrology to be similar to our study. In the previous works use was made of the absolute sphericity measurement [16], the microlens form error and wavefront aberration measurement [17] to obtain the interference characteristics of the reflected light. The above proved to be effective to measure some parameters. So these methods for studying the interference characteristics of the cat-eye reflected light will be effective and direct to get and measure some parameters such as the incidence angle of the detected laser beam entering the target optical lens.

Therefore, the goal of our research was to derive formulas describing the interference of the cat-eye reflected light with the reference incidence light. It is a nonparaxial propagation for the detected laser beam entering the target optical lens, so the Fresnel diffraction theory is not precise to be used to calculate the diffraction process. Under nonparaxial condition, the Kirchhoff formula, Rayleigh–Sommerfeld formula and angular spectrum diffraction formula are all veracious and can be calculated by using the fast Fourier transform algorithm. Compared to the other two formulas, the calculation speed of angular spectrum diffraction formula is faster and the sampling condition can be satisfied more easily [18, 19]. Therefore, we will perform our research based on the angular spectrum theory [18, 19] and the idea that the light-waves from a tilted and defocused cat-eye optical lens when irradiated by laser beam can be regarded as an off-axis spherical wave. We further show proofs of our theory through numerical computation, within the relationships governing the variation of the interference characteristics within parameters including the following: incidence angle, tilted angle of the moving mirror, and focal shift, will be derived. The relationships will be experimentally validated. Descriptions will be given to show how to estimate and deduce the tilted angle of the cat-eye target.

2. Theoretical analysis

Figure 1 shows the process of the cat-eye reflected light interfering with the reference incidence light. Because of the back-reflected character of the cat-eye reflected light, its optical pathway is superposed on the incidence light, so a split prism and a moving mirror are placed. The thin beam produced by the laser passes a beam expander (BE) and is collimated by lens 1, and then is separated into two beams by the split prism. The reflected light beam propagates to the moving mirror which is used to adjust the incidence reference light, then is reflected and passed through the split prism, finally propagates to the receiving screen. The transmitted light propagates to the cat--eye system which can be simplified to a lens and a reflector on its focal plane. It is reflected along the entrance way, then is reflected by the split prism, finally propagates to the receiving screen, on which the cat-eye reflected light will interfere with the reference incidence light. Here, the split prism is a cube and the influence of its machining error on the interference light can be ignored.

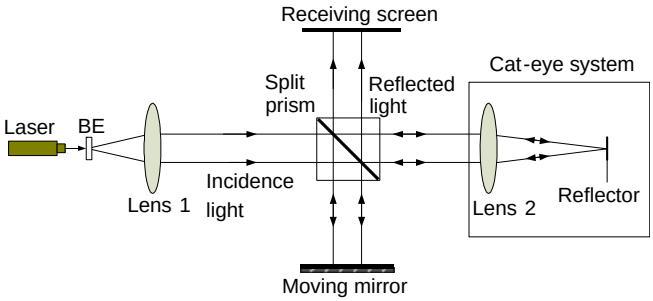

Fig. 1. Sketch map of the cat-eye effect reflected light interfering with the reference incidence light.

Figure 1 allows the study of the propagation of the cat-eye reflected light to begin. In order to analyze the process of the beam propagating in the cat-eye system expediently, the cat-eye system can be expanded to a combination with an aperture at the reflector plane and two lenses: lens 2 in Fig. 1 and its symmetrical lens 2′ about the reflector plane, which can be seen in Fig. 2. Because the incidence beam has been expanded, the incidence light before the cat-eye system can be regarded as a planar wave, so only four incidence rays are drawn in Fig. 2. Under the given conditions, using a laser beam to detect an optical lens, the axis of the detected laser and the optical axis of the target optical lens are not matched. Here, z is the axis of the detected laser, z' is the optical axis of the cat-eye system, θ is the tilted angle of the cat-eye system in y direction, namely the incidence angle of the detected laser. Assume that O is the center of lens 2 as the axis of origin, f is the focus of lens 2 and lens 2′, δ is the distance between the reflector and the focal plane defined as focal shift (its value is "–" when the reflector is between the focal plane and lens 2, and "+" contrarily), D is the effective diameter of lens 2 and lens 2′, L is the distance between O and the receiving screen.

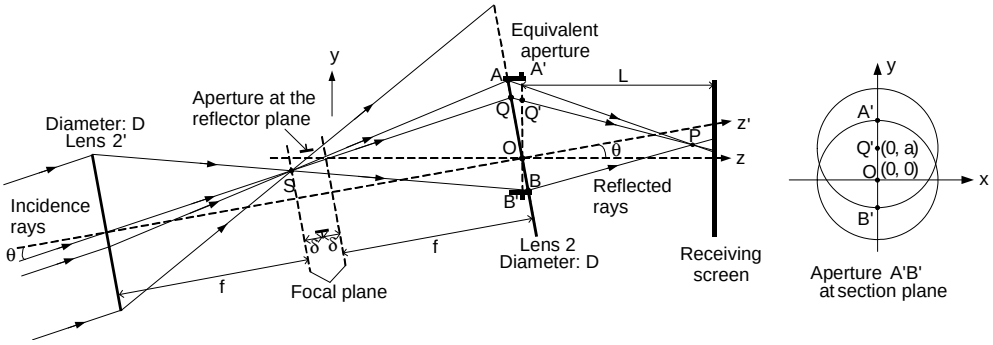

Fig. 2. Propagation process of cat-eye effect reflected light from a tilted and defocused optical lens.

According to geometry optics theory, all of the incidence rays will be focused at point *S* on the focal plane of lens 2′, then propagate through the aperture at the reflector plane and propagate onto lens 2. So, all the reflected rays before lens 2 can be seen as a tilted spherical wave from the light source *S*. Furthermore, according to the transform rules of spherical wave passing through thin-lens, the reflected rays after lens 2 can also be regarded as a tilted spherical wave which will focus at point *P*, as the location of the sphere center. We set the coordinate of *P* to be (x_0, y_0, z_0), according to the object-image relation of thin-lens we can get

$$x_0 = 0, \quad y_0 = f\sin\theta, \quad z_0 = \frac{f(f + 2\delta\cos^2\theta)}{2\delta\cos\theta} \tag{1}$$

From Eq. (1) we know that this spherical wave after lens 2 is an off-axis and tilted spherical wave, and its optical field at plane $z = 0$ can be expressed as follows [20]

$$E_0(x, y, 0) = \exp\left\{-ik\left[\frac{x^2 + (y - y_0)^2}{2z_0} + z_0\right]\right\} \tag{2}$$

where $k = 2\pi/\lambda$ is the wave number, λ is the wavelength. Especially, when $\delta = 0$, the spherical wave becomes a planar wave, $E_0(x, y, 0) = 1$.

Back to Fig. 2, we know that because of the incline of lens 2, only the reflected rays between *A* and *B* can pass lens 2 and propagate back along the entrance way in *y* direction, as a tilted aperture is located at lens 2. The tilted aperture *AB* can be rotated to *A*′*B*′ which is upright to *z* axis, their diffraction effect can be equivalent to that of the two apertures of lens 2′ and lens 2 when θ is not very large. In *x*–*y* plane, the aperture *A*′*B*′ is the intersection of two ellipse apertures, whose long radiuses are $D/2$ in *x* direction, short radiuses are $(D\cos\theta)/2$ in *y* direction, and their center coordinates are (0, 0) and (0, *a*), respectively. So the aperture function of *A*′*B*′ can be written as follows

$$J(x, y) = A(x, y)B(x, y) \tag{3}$$

and

$$A(x, y) = \begin{cases} 1, & x^2 + y^2\cos^2\theta \le D^2/4 \\ 0, & x^2 + y^2\cos^2\theta > D^2/4 \end{cases} \tag{4}$$

$$B(x, y) = \begin{cases} 1, & x^2 + (y - a)^2\cos^2\theta \le D^2/4 \\ 0, & x^2 + (y - a)^2\cos^2\theta > D^2/4 \end{cases} \tag{5}$$

where $a = 2(f - \delta)\sin\theta$. So the optical field at $z = 0$ after aperture $A'B'$ can be expressed by equation

$$E_1(x, y, 0) = J(x, y)\, E_0(x, y, 0) \tag{6}$$

Based on the theory of angular spectrum, $E_1(x, y, 0)$ can be regarded as the summation of a series of basal functions with different special frequencies which can be denoted as $\exp[i2\pi(f_x x + f_y y)]$, and its Fourier transfer, namely its angular spectrum, can be written as

$$U_1(f_x, f_y) = \iint_{-\infty}^{+\infty} E_1(x, y, 0)\exp\left[-i2\pi(f_x x + f_y y)\right]\mathrm{d}x\mathrm{d}y \tag{7}$$

where f_x and f_y are the special frequencies of the angular spectrum.

According to the diffraction formula of angular spectrum, the angular spectrum of the optical field at the receiving screen can be given by

$$U_2(f_x, f_y) = U_1(f_x, f_y)\, H(f_x, f_y) \tag{8}$$

where

$$H(f_x, f_y) = \exp\left[ikL\sqrt{1 - (\lambda f_x)^2 - (\lambda f_y)^2}\right] \tag{9}$$

is the standard diffraction transfer function, which is a compound function with module 1. So the optical field at the receiving screen can be expressed as

$$E_2(x, y, z) = \iint_{-\infty}^{+\infty} U_2(f_x, f_y)\exp\left[i2\pi(f_x x + f_y y)\right]\mathrm{d}f_x\mathrm{d}f_y \tag{10}$$

Now let us return to the analysis of the optical field of the reference incidence light. According to interference theory, a necessary condition for the interference of two beams is that a stable optical difference surface should be formed at the receiving screen [21]. If $\delta = 0$, the cat-eye reflected light can be regard as a planar wave. If the reference incidence light is also a planar wave, the interference effect will not occur. Furthermore, in practical conditions, the reference incidence light cannot be

a perfect planar wave, because the collimate error and the diffraction effect of the effective aperture of lens 1 is always existent. Therefore, the reference incidence light should be regarded as a spherical wave, too. We assume δ_0 is the equivalent focus shift of this spherical wave, f_0 is the equivalent focus, D_0 is the effective diameter of lens 1, L_0 is the total propagation distance of the reference incidence light from lens 1 to the receiving screen, L' is the distance between the moving mirror and the receiving screen, ε is the tilted angle of the moving mirror. Here, ε is difficult to be adjusted to zero and can be used to control the interference light distribution on the receiving screen.

Similarly, the deduced process of the cat-eye reflected light, the optical field of the reference incidence light on the receiving screen can be given by the formula

$$E_3(x, y, z) = W(y)\iint_{-\infty}^{+\infty} H'(f_x, f_y) \times F\left\{C(x, y)\exp\left[-ik\left(\frac{x^2 + y^2}{2z_0'} + z_0'\right)\right]\right\} \times \\ \times \exp\left[i2\pi(f_x x + f_y y)\right] \mathrm{d}f_x \mathrm{d}f_y \tag{11}$$

where

$$z_0' = \frac{f_0(f_0 + 2\delta_0)}{2\delta_0} \tag{12}$$

$$C(x, y) = \begin{cases} 1, & x^2 + \left[y - L'\tan(2\varepsilon)\right]^2 \le D_0^2/4 \\ 0, & x^2 + \left[y - L'\tan(2\varepsilon)\right]^2 > D_0^2/4 \end{cases} \tag{13}$$

$$H'(f_x, f_y) = \exp\left[ikL_0\sqrt{1 - (\lambda f_x)^2 - (\lambda f_y)^2}\right] \tag{14}$$

and

$$W(y) = \exp\left\{ik\tan(2\varepsilon)\left(y + \frac{D_0}{2}\right)\right\} \tag{15}$$

is the phase difference function brought by the incline of the moving mirror in y direction. So, the interference optical field on the receiving screen can be written as

$$E(x, y, z) = E_2(x, y, z)\exp(i\pi) + E_3(x, y, z) \tag{16}$$

Here, $\exp(i\pi)$ is the phase difference brought by the peculiar reflected form of cat-eye system, and the interference intension distribution is given by

$$I(x, y, z) = E(x, y, z)\, E^*(x, y, z) \tag{17}$$

Here, $E^*(x, y, z)$ is the conjugated function of $E(x, y, z)$. So the phase function of the interference optical field can be expressed as

$$\varphi(x, y) = \cos\left[\operatorname{atan}\left(-i\frac{E_3 - E_3^*}{E_3 + E_3^*}\right) - \operatorname{atan}\left(-i\frac{E_2 - E_2^*}{E_2 + E_2^*}\right) + \frac{\pi}{2}\left(\frac{|E_2 + E_2^*|}{E_2 + E_2^*} - \frac{|E_3 + E_3^*|}{E_3 + E_3^*}\right)\right] \tag{18}$$

What is more, based on the geometrical optical path theory of interference [22], after straightforward integration, the geometrical phase function can be written as

$$\varphi'(x, y) = \cos\left[k\sqrt{(L - L_0 - z_0)^2 + x^2 + (y - y_0)^2} + ky\tan(2\varepsilon) + \pi\right] \tag{19}$$

In the following numerical computation, we will study whether the geometrical phase function can be used to replace the real diffractive phase function or not.

3. Numerical computation

Figure 3 illustrates the interference intensity distributions on the receiving screen when θ is variable. Here, we set $\lambda = 0.6328$ μm, $L = 5$ m, $f = 300$ mm, $\delta = -5$ mm, $L_0 = 2$ m, $L' = 0.6$ m, $f_0 = 300$ mm, $D_0 = D = 15$ mm, $\delta_0 = 1$ μm, $\varepsilon = 0°$, the screen size is 22×22 mm, the sampling number is 512×512, and the on-axis intensity at lens 2 namely $I_0(0, 0, 0) = 1$, all the values are relative to $I_0(0, 0, 0)$, so no values are labeled.

From Fig. 3 we can see a series of thin-inside and thick-outside circles when $\theta = 0°$. The interference circles gradually move outwards along with the increase of θ, and the profile of all the interference circles becomes smaller and broken because of the limitation of aperture $A'B'$. The widths of the interference fringes and spaces between two fringes are stable when θ is variable. All the interference fringes have the same curvature center.

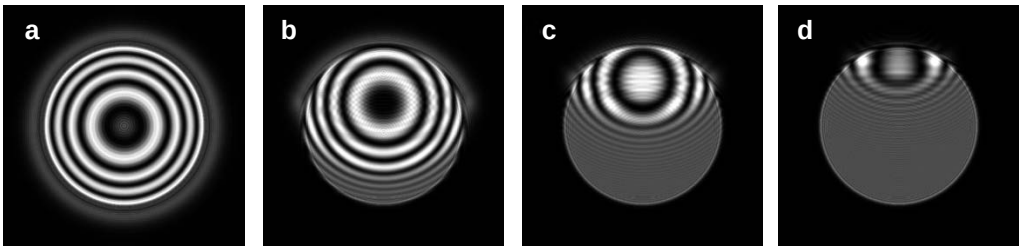

Fig. 3. Interference intensity distributions on the screen when θ is variable: $\theta = 0°$ (**a**) $\theta = 0.4°$ (**b**), $\theta = 0.8°$ (**c**), and $\theta = 1.1°$ (**d**).

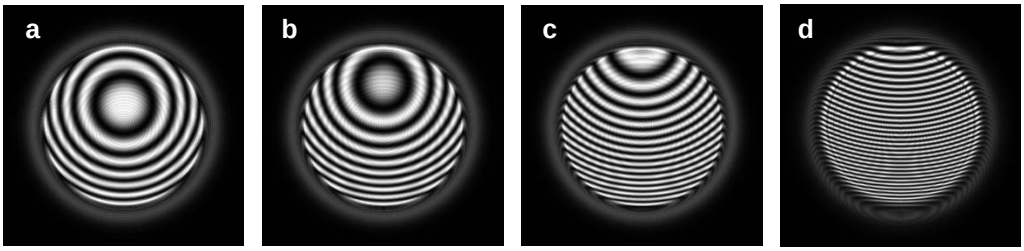

Fig. 4. Interference intensity distributions on the screen when ε is variable: $\varepsilon = 0.005°$ (**a**), $\varepsilon = 0.01°$ (**b**), $\varepsilon = 0.02°$ (**c**) and $\varepsilon = 0.04°$ (**d**).

Then set $\theta = 0°$. Figure 4 illustrates the interference intensity distributions on the receiving screen when ε is variable. We can see that the interference circles gradually move outwards which is similar to what we have seen in Fig. 3, but the profile of all the interference fringes is circular constantly, the number of the interference fringes becomes larger and the spaces between two fringes become smaller along with the increase of ε. When $\varepsilon > 0.02°$, the curvature center of the interference fringes is outside of the receiving aperture, so a series of curving thick-upside and thin-downside fringes can be seen.

From the analysis above we have proven that it is the curvature center, the number of the interference fringes, and the profile of all the interference fringes that contain the maximal amount of information about θ and ε. It must be noted that the edge of the profile of all the interference fringes is distorted when θ is variable, so it is difficult to test the value of θ by testing the size of the profile. In order to get an exact relationship of the number of the interference fringes and the curvature centers with θ and ε, it is necessary to be apply the geometrical optical path theory. Figure 5 shows the real diffractive phase function expressed by Eq. (18) and the geometrical phase function expressed by Eq. (19) when $x = 0$, $\theta = 0°$, $\varepsilon = 0.01°$. From Fig. 5 we can see

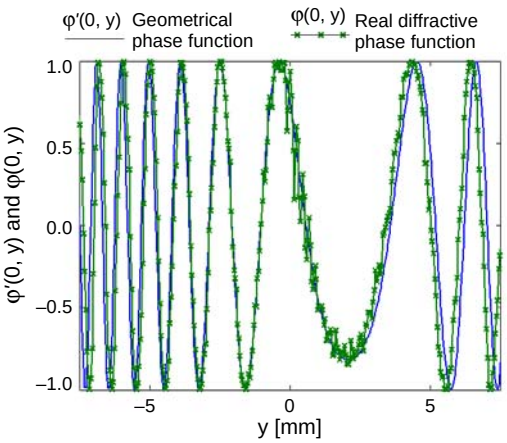

Fig. 5. Geometrical phase function and real diffractive phase function.

that the geometrical phase function is very close to the real diffractive phase function when y is in the range of $(-D/2, D/2)$. Although some departures exist when the absolute value of y is close to $D/2$ and an initial phase difference exists, the number of the peak values and the spaces between two neighboring peak values are almost the same. So the geometrical phase function can replace the real diffractive phase function, and the geometrical optical path theory can be used when L is not a high value.

Therefore, we assume that the apertures of the cat-eye system and lens 1 are infinite. Without the restriction of apertures, the interference process of the cat-eye reflected light within the reference incidence light can be considered as an interference of an off-axis and tilted spherical wave with a planar wave. Based on Eqs. (1) and (19), the y coordinate of the curvature center of the interference fringes can be calculated

$$Y_0 = f\tan\theta + (L - L_0 - z_0)\tan(2\varepsilon) \tag{20}$$

The results obtained using Eq. (20) can be proven to accord with the results obtained with the use of the real diffraction field distribution through numerical computation. So, all the interference fringes have the same curvature center Y_0 no matter whatever ε and θ are. Figure 6 shows the effect of ε and θ on Y_0. We have measured that the curvature center coordinates of all the fringes are proportional to ε and θ. The increasing speed of Y_0 as controlled by ε is much faster than that controlled by θ. This is because the cat-eye system possesses a low sensitivity to the incidence angle, the effect of θ on the cat-eye reflected light is just equal to the effect of the off-axis size y_0 which has been given in Eq. (1).

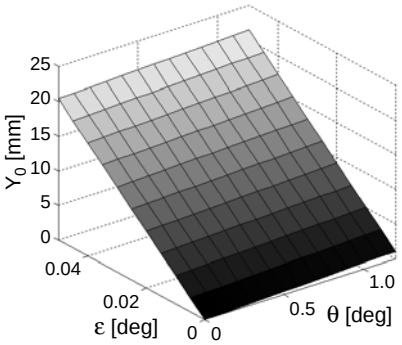

Fig. 6. Effect of ε and θ on the curvature center coordinate of the interference fringes.

Similarly, following the analysis of Eq. (20), the number of the interference fringes in y direction can be written as

$$N = \frac{\left|\sqrt{(L - L_0 - z_0)^2 + (0.5D - y_0)^2} - \sqrt{(L - L_0 - z_0)^2 + y_0^2} + (Y' + 0.5D)\tan(2\varepsilon)\right|}{\lambda} \tag{21}$$

Here, Y' is the lesser value of Y_0 and $0.5D$, $x = 0$. When $Y_0 \le 0.5D$, N means the number of the fringes from the curvature center with a y coordinate of Y_0 to the down edge

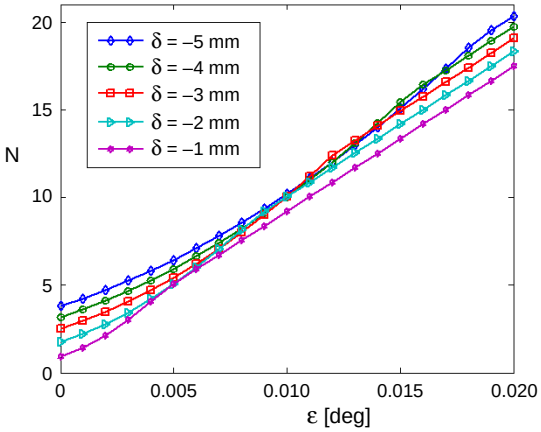

Fig. 7. Effect of ε on the number of the interference fringes.

with a y coordinate of $0.5D$; when $Y_0 \geq 0.5D$, N means the number of all the fringes. From Eq. (21) we know that N is primarily influenced by ε and δ, but almost independent of θ.

Figure 7 shows the effect of ε on N with several different values of δ. We can see that the number of the interference fringes increases along with the increase of ε, but the relation is not linear. δ is a necessary condition for the interference to occur; if the absolute value of δ is smaller than 1 mm, the number of the interference fringes will be less than 1 and it will be difficult to be see and test the interference fringes. Under such conditions, the number of the interference fringes can be raised by adjusting the value of ε. Therefore, by testing the number of the fringes, the curvature of the interference fringes and the tilted angle of the moving mirror, the tilted state of the cat-eye system can be deduced and estimated.

4. Experiment

The experimental equipment shown in Fig. 8 is developed from Fig. 1. The reflector in the focal plane in the cat-eye system in Fig. 1 is replaced by a mirror instead. Two circular apertures with a diameter of 15 mm are placed close to the surface of lens 1 and lens 2. The incidence thin beam is produced by a He-Ne laser whose power is 5 mW. The receiving screen in Fig. 1 is replaced by lens 3 with a diameter of 22 mm. The reflected spot received by lens 3 is focused on the CCD which is placed nearby the focal plane of lens 3 and has 576×576 pixels, the spot profile will not change so long as lens 3 has little aberration and the optical pathway has little difference. Finally, spots on the CCD are collected by a data collection card and transmitted to computer. The incidence angle namely the tilted angle of the cat-eye system can be adjusted by a three dimensional adjust system. Other diameters in the experiments are the same as the setting values in numerical computation.

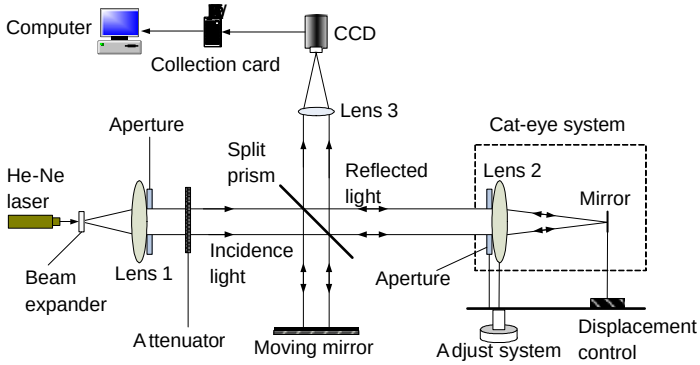

Fig. 8. Sketch map of experimental setup.

Figure 9 shows the interference intensity distributions on the CCD when θ is variable. We can see that the rules are almost accordant with the results shown in Fig. 3. The spots obtained in the experiment have some distortions because of the adjustment error of the optical path and the non-uniformity of the incidence laser beam. The interference fringes are not clear enough to be distinguished especially when θ is close to the critical viewing angle of the cat-eye system. The edges of the profiles of all the interference fringes are not clear and smooth compared to that shown in Fig. 3, the reason being that the edges of the two circular apertures which are placed before

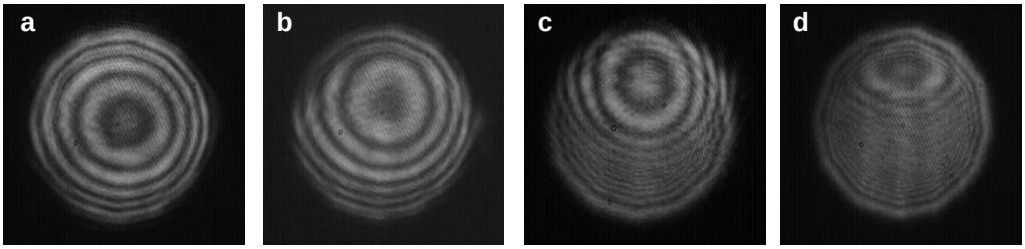

Fig. 9. Interference intensity distributions on CCD when θ is variable: $\theta = 0°$ (**a**), $\theta = 0.4°$ (**b**), $\theta = 0.8°$ (**c**) and $\theta = 1.1°$ (**d**).

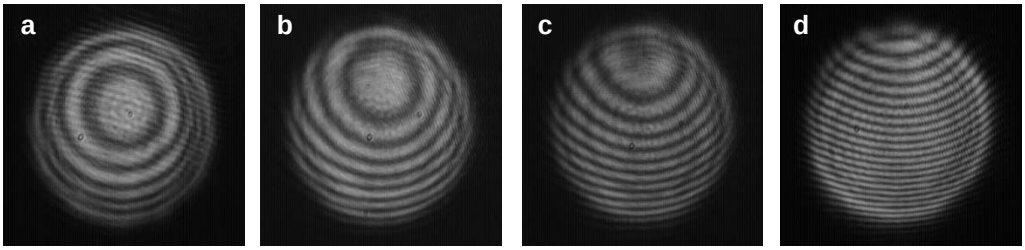

Fig. 10. Interference intensity distributions on CCD when ε is variable: $\varepsilon = 0.005°$ (**a**), $\varepsilon = 0.01°$ (**b**), $\varepsilon = 0.02°$ (**c**) and $\varepsilon = 0.04°$ (**d**).

lens 1 and lens 2 are not smooth, so the verge diffraction is stronger. What is more, the widths of the diffraction fringes are larger than those obtained in numerical computation, and the diffraction fringes are easily promiscuous to the interference fringes. However, the curvatures of the diffraction fringes and the interference fringes are different, so the profile verge of all the interference fringes could be distinguished through testing the curvatures of the fringes.

The same phenomenon can be seen in Fig. 10, which shows the interference intensity distributions on the CCD when ε is variable, and can validate the rules observed in Fig. 4. Similarly, because of the stronger verge diffraction of the apertures before lens 1 and lens 2, the number of the interference fringes is smaller than that obtained in numerical computation, and the difference becomes greater along with the increase of ε. The distributions of Figs. 10**a** and 9**b** are very similar, under this condition, the difference could be distinguished by testing the curvatures of all the fringes, the results show that there are some diffraction fringes whose curvatures are not the same as those of the interference fringes in Fig. 9**b**, but there are no diffraction fringes because the curvatures of all the fringes in Fig. 10**b** are the same.

Now, we give an example of how to estimate and deduce the tilted angle of the cat-eye target, in other words, how to test the value of θ. Assume the true value of θ is 0.8°, but it is unknown before testing. The test and calculation processes are as follows.

At first, by adjusting the value of ε, we get the interference intensity distribution with the least interference fringes, which is shown in Fig. 9**c**. From the simulation and experimental results we know that ε is zero now. Second, we test the curvatures and positions of the interference fringes, then deduce the position of their curvature center, namely the value of y_0. Now, θ could be calculated directly by using Eq. (20), but the error is very large, so ε should be adjusted to get a larger number of interference fringes. Then, when ε is not zero, based on Eq. (21) and by testing the value of N, we can obtain the value of z_0. Finally, based on Eq. (20) and by testing the value of Y_0, we can finally calculate the value of θ.

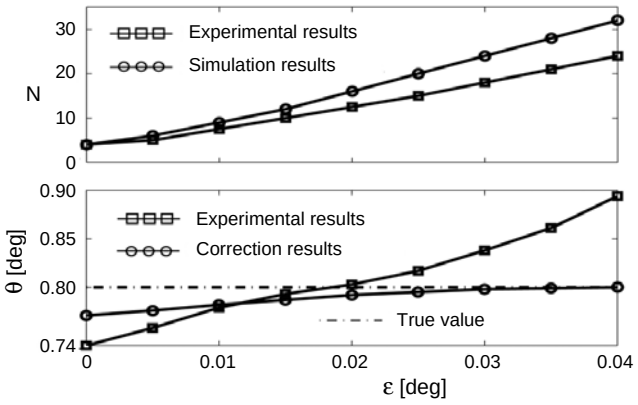

Fig. 11. The testing values of N and θ and their errors relative to the simulation results.

The tested and calculated results are shown in Fig. 11. We can see that the testing error is quite large when ε is zero. It decreases along with the increase of ε when ε is not greater than 0.018°, then increases when ε continues to increase. It is inconsistent with our expectations, that is, because the testing errors of N between the experimental results and the simulation results are large, and increase along with the increase of ε. So, the testing values of N should be corrected, from the correction results we can see that the testing errors will decrease along with the increase of ε all the time. Therefore, these experimental results should be disposed further to get accurate values of Y_0 and N in the following research.

5. Conclusions

In order to confirm the dangerous state of the optical target which has been detected by the active laser detection system, and make clear which location is being watched, it is necessary to get definite parameters especially the tilted angle of the target optical lens. The study on the interference characteristics of the cat-eye reflected light provides an effective method to get and measure the incidence angle of the detected laser beam entering the target optical lens. Therefore, in this paper, the authors study the interference characteristics of the cat-eye reflected light with the reference incidence light, especially the rules of the interference field distribution effected by the incidence angle of detected laser and the tilted angle of the moving mirror. The results obtained in numerical computation and experiment are proven to be consistent. In conclusion, in the finite aperture of the receiving system, the interference process is proven to be equivalent to that of an off-axis and tilted spherical wave with a planar wave. The coordinates of the curvature center of the interference fringes are proportional to the incidence angle and the tilted angle of the moving mirror. If the number of the interference fringes is too small to test when the focal shift is too small, the problem can be solved by adjusting the tilted angle of the moving mirror. Similarly, if the moving mirror is replaced by a spherical mirror, the number of the interference fringes can be raised, too. So the tilted state of the cat-eye system can be deduced and estimated. In the following research, the results obtained in this paper will find the application, and a recognition system aimed at the optical target will be founded in nearby distance.

Acknowledgements – This work was supported by the National Defense Pre-Research Foundation of China under Grant No. 513210902. Furthermore, many thanks to our American friend Mr. Brian McNally for his assistance in careful modification of the English expression of our manuscript.

References

[1] LECOCQ C., DESHORS G., LADO-BORDOWSKY O., MEYZONNETTE J.L., *Sight laser detection modeling*, Proceedings of SPIE **5086**, 2003, pp. 280–286.

[2] HAN Y., WU J., YANG C.P., HE W.G., XU G.Y., *Propagation studying in cat-eye system for the beam affected by atmospheric turbulence*, Proceedings of SPIE **6795**, 2007, p. 67952O.

[3] ZHAO Y.Z., SUN H.Y., SONG F.H., TANG L.M., WU W.W., ZHANG X., GUO H.C., *Research on the mechanism of reflection characteristics of laser irradiation on the cat eye optical lens*, Acta Physica Sinica **57**(4), 2008, pp. 2284–2294, (in Chinese).

[4] ZHAO Y.Z., SUN H.Y., SONG F.H., DAI D.D., *Propagation properties of Gaussian beams through cat eye optical lens with center shelter*, Optik **121**(24), 2010, pp. 2198–2201.

[5] BIERMANN M.L., RABINOVICH W.S., MAHON R., GILBREATH G.C., *Design and analysis of a diffraction--limited cat's-eye retroreflector*, Optical Engineering **41**(7), 2002, pp. 1655–1660.

[6] LIN Y.B., ZHANG G.X., LI Z., *An improved cat's-eye retroreflector used in a laser tracking interferometer system*, Measurement Science and Technology **14**(6), 2003, pp. N36–N40.

[7] DIMAKOV S.A., KLIMENTEV S.I., KHLOPONINA I.V., *Cavity with a cat's-eye reflector based on elements of conical optics*, Journal of Optical Technology **69**(8), 2002, pp. 536–540.

[8] XU Z.G., ZHANG S.L., LI Y., DU W.H., *Adjustment-free cat's eye cavity He-Ne laser and its outstanding stability*, Optics Express **13**(14), 2005, pp. 5565–5573.

[9] REN D.M., LAWTON K.M., MILLER J.A., *Application of cat's-eye retroreflector in micro-displacement measurement*, Precision Engineering **31**(1), 2007, pp. 68–71.

[10] RABINOVICH W.S., MAHON R., GOETZ P.G., SWINGEN L., MURPHY J., FERRARO M., BURRIS H.R., SUITE M., MOORE C.I., GILBREATH G.C., BINARI S., KLOTZKIN D., *45 Mbps cat's eye modulating retro--reflector link over 7 Km*, Optical Engineering **46**(10), 2007, p. 104001.

[11] GOETZ P.G., RABINOVICH W.S., BINARI S.C., MITTEREDER J.A., *High-performance chirped electrode design for cat's eye retro-reflector modulators*, IEEE Photonics Technology Letters **18**(21), 2006, pp. 2278–2280.

[12] RABINOVICH W.S., MAHON R., GOETZ P.G., WALUSCHKA E., KATZER D.S., BINARI S.C., GILBREATH G.C., *A cat's eye multiple quantum-well modulating retro-reflector*, IEEE Photonics Technology Letters **15**(3), 2003, pp. 461–463.

[13] ZHAO Y.Z., SUN H.Y., SONG F.H., GU S.L., *Laser reflection characteristics of "cat eye effect" of photoelectric equipment*, Proceedings of the 7th International Symposium on Test and Measurement, Zhongbei University, Beijing, August 5–8, 2007, pp. 2991–2994.

[14] ZHAO Y.Z., SUN H.Y., SONG F.H., DAI D.D., *Propagation properties of oblique and off-axial Gaussian beams passing through cat-eye optical lens*, Acta Optica Sinica **29**(9), 2009, pp. 2252–2256, (in Chinese).

[15] ZHAO Y.Z., SONG F.H., SUN H.Y., ZHANG X., GUO H.C., XU J.W., *Laser reflection characteristics of cat eye effect of Cassegrain lens*, Chinese Journal of Lasers **35**(8), 2008, pp. 1149–1155, (in Chinese).

[16] ELSSNER K.E., BUROW R., GRZANNA J., SPOLACZYK R., *Absolute sphericity measurement*, Applied Optics **28**(21), 1989, pp. 4649–4661.

[17] GOMEZ V., GHIM Y.S., OTTEVAERE H., GARDNER N., BERGNER B., MEDICUS K., DAVIES A., *Thienpont H.,. Micro-optic reflection and transmission interferometer for complete microlens characterization*, Measurement Science and Technology **20**(2), 2009, p. 025901.

[18] LI J.C., PENG Z.J., FU Y.C., *Diffraction transfer function and its calcution of classic diffraction formula*, Optics Communications **280**(2), 2007, pp. 243–248.

[19] LI J.C., *FFT computation of angular spectrum diffraction formula and its application in wavefront reconstruction of digital holography*, Acta Optica Sinica **29**(5), 2009, pp. 1163–1167, (in Chinese).

[20] LI M., ZHANG D., WANG Z.Y., GAO X.Y., *Diffraction mode of axicon for tilted spherical wave beam*, Acta Optica Sinica **28**(4), 2008, pp.773–778, (in Chinese).

[21] LIANG Q.T., *Physical Optics*, 3th Edition, Publishing House of Electronics Industry Press, Beijing, 2008, pp.75–78, (in Chinese).

[22] ZENG X.H., WU F.T., LIU L., *The description of bottle beam based on the interferential theory*, Acta Physica Sinica **56**(2), 2007, pp. 791–797, (in Chinese).

Received September 25, 2010
in revised form December 14, 2010